Available online at www.sciencedirect.com
ScienceDirect
Polymer 48 (2007) 5497–5506
polymer
www.elsevier.com/locate/polymer

A kinetic model for the chemical degradation of perfluorinated sulfonic acid ionomers: Weak end groups versus side chain cleavage

Tao Xie [a,*], Charlene A. Hayden [b]

[a] *Materials and Processes Lab, General Motors Research and Development Center, Mail Code: 480-106-710, 30500 Mound Road, Warren, MI 48090, USA*
[b] *Chemical and Environmental Sciences Lab, General Motors Research and Development Center, Mail Code: 480-106-320, 30500 Mound Road, Warren, MI 48090, USA*

Received 8 June 2007; received in revised form 13 July 2007; accepted 21 July 2007
Available online 26 July 2007

Abstract

The durability of proton exchange membranes (PEMs) is a critical factor in the future commercial success of hydrogen fuel cell technology. Presently, the favored PEM material is made of perfluorinated sulfonic acid (PFSA) ionomers. Current efforts to improve PFSA durability are hindered by the lack of thorough understanding of the chemical mechanism by which PFSA degrades. In this paper, the PFSA chemical degradation mechanism is reviewed which incorporates two possibilities for initiation along the PFSA polymer: weak polymer end groups versus side chain cleavage. A kinetic model is developed which quantitatively distinguishes between these two degradation initiation mechanisms. Experimentally, degraded PFSA samples were obtained under both fuel cell and ex situ Fenton's test conditions, and infrared spectroscopy (IR) was used to measure the relative concentration of carboxylic acid end groups on the degraded polymer chains. The IR data, coupled with the corresponding ionomer fluoride loss data, validate the kinetic model and allow calculation of the kinetic constants which distinguish between the two degradation initiation mechanisms. Theoretical case studies are also included to illustrate the usefulness of the kinetic model.

Keywords: Proton exchange membrane; Ionomer; Degradation

1. Introduction

Hydrogen fuel cell technology has been perceived by many as the next energy revolution. Among the critical issues for its future commercial success is the chemical durability of the proton exchange membranes (PEMs). PEM chemical durability depends largely on the nature of the material and the conditions under which the fuel cell is operated. In terms of the PEM material, perfluorinated sulfonic acid (PFSA) ionomers are the heavily favored choice at the present time [1,2]. A typical PFSA is Nafion®, with its structure shown in Scheme 1. Although a large number of hydrocarbon-based PEM materials have been developed [3], thus far none has shown reliable durability matching that of PFSA. While the search for alternative PEM materials continues, an important area of development focuses on further improving PFSA durability.

Given the technological importance of PFSA and the fact that both PFSA and hydrogen fuel cells have been around for many years, the progress in improving the chemical durability of PFSA has been rather limited. This rate of progress is limited largely due to the lack of complete understanding of

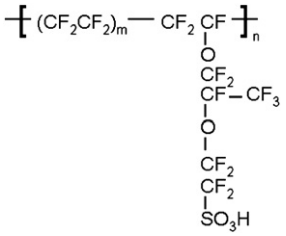

Scheme 1. Structure of Nafion® ($m = 6.56$ for an equivalent weight (EW) of 1100).

* Corresponding author. Tel.: +1 586 947 2471; fax: +1 586 986 1207.
E-mail address: tao.xie@gm.com (T. Xie).

0032-3861/$ - see front matter © 2007 Elsevier Ltd. All rights reserved.
doi:10.1016/j.polymer.2007.07.043

the fundamental mechanism by which PFSA chemically degrades. Various possible degradation environments for PFSA include degradation in both ex situ tests and in situ fuel cell tests. Several ex situ tests (e.g. Fenton's test [4] and more recently H_2O_2 flow cell test [5]) are often used to accelerate the degradation to facilitate PEM durability evaluation. These ex situ tests are quick and require only simple experimental setups. At debate, however, is how well these ex situ accelerating tests correlate to PFSA degradation in real fuel cells [1,6,7]. Fundamentally, the debate translates into whether PFSA chemical degradation in ex situ tests follows the same mechanism as in fuel cells.

It is generally accepted that PFSA degradation proceeds via an unzipping mechanism through the carboxylic acid end groups in all of the afore-mentioned tests (in situ fuel cell, Fenton's test, and H_2O_2 flow cell test) [1,4–7]. What is under debate is where these carboxylic acid end groups originate. One widely accepted mechanism points to the weak polymer end groups as the initial source of carboxylic acid end groups [1,4–7]. Another mechanism suggests that the PFSA side chain is the source [1,5]. This second mechanism (the so-called "side chain cleavage mechanism"), if it occurs, is much more detrimental compared to the first mechanism. On the one hand, it reduces the polymer molecular weight (or chain length) in a very drastic fashion [5]; on the other hand, it creates additional carboxylic acid end groups on the polymer which accelerate the degradation rate [5].

For Fenton's tests, there is strong evidence in the literature suggesting that the weak polymer end groups in a PFSA polymer are the dominant source of the carboxylic acid end groups [6,7]. Recently, the occurrence of the PFSA side chain cleavage reaction in H_2O_2 flow cell tests was reported, in addition to the weak end group reaction [5]. What remains unknown, however, is the ultimate question of whether the side chain cleavage reaction occurs under fuel cell conditions.

The complexity of fuel cell systems makes it difficult to study PFSA chemical degradation in situ in such an environment [8]. In this paper, we use Nafion® ionomer with an equivalent weight (EW) of 1100 as a representative of PFSA ionomers and develop a kinetic model that can be used as a tool to elucidate the initiation mechanisms for PFSA chemical degradation in various degradation environments including fuel cells. This model allows us to quantitatively determine whether and how degradation conditions (e.g. fuel cell operating conditions) affect the extent of side chain cleavage. Ultimately, the potential impact of this work lies in: (1) confirming the relevance/irrelevance of the accelerating ex situ tests and (2) providing guidance in improving PFSA durability through purposeful molecular design of new PFSA materials.

2. Experimental section

2.1. Sample preparation

A Nafion® membrane of equivalent weight (EW) of 1100 was degraded under the following Fenton's test conditions: 95 °C, 30% H_2O_2, 4 ppm Fe (II), 48 h.

Two membrane electrode assemblies (MEAs) were constructed with N112 (extruded) and equal Pt catalyst loadings of 0.4 mg/cm^2 on both anode and cathode. Nafion ionomer of equivalent weight (EW) of 1100 was used in the catalyst layer. The two MEAs were subjected to fuel cell degradation (conducted at General Motors Fuel Cell Activities) using 50 cm^2 cells under the following operating conditions: temperature of 80 °C, current density of 0.02 A/cm^2, relative humidity of 50% for both anode and cathode inlet gases. The fuel cell running hours for the two MEAs were 100 and 200, respectively. After the fuel cell runs, small pieces (1 cm × 2 cm) were cut from each degraded MEA.

The Fenton's tested membrane and the fuel cell-degraded MEAs were soaked overnight in 0.1 N KOH in order to assure complete ion exchange of the carboxyl groups to the K^+ acid salt species. These ion-exchanged samples were then soaked in deionized water for up to 3 days, during which the water was replaced 2–3 times per day until a constant pH was reached. The samples were let dry under ambient conditions for a minimum of 4 days and cut into 10 μm thick cross-sections using a dry microtome procedure.

2.2. Micro-infrared analysis

A small piece (~1 mm in length) of each microtomed cross-section was cut with a razor blade and transferred to the top surface of a diamond anvil cell. Infrared spectra were obtained in transmission mode using a ThermoNicolet Continuum microscope accessory connected to a ThermoNicolet Magna 760-IR spectrometer. The sample aperture size for transmission was 25, 50, or 100 μm × 100 μm, and 32 scans were signal-averaged at 4 cm^{-1} spectral resolution. A minimum of 10 individual spectra were collected for each degraded sample by translating the diamond anvil cell to a different location along the microtomed cross-section piece. Baseline corrected peak heights were calculated from a "macro" program using ThermoNicolet's Macros Basic software package.

3. Results and discussion

3.1. Review of degradation mechanism

3.1.1. Degradation initiation via weak end groups

The widely accepted mechanism by which PFSA degrades starts from the weak polymer end groups [1,4–7]. These weak end groups, presumably non-perfluorinated groups [9], react with hydroxyl radicals to yield carboxylic acid end groups as shown in Scheme 2.

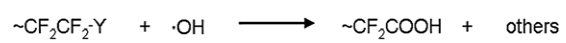

Scheme 2. Formation of carboxylic acid end groups from non-perfluorinated weak end groups (represented as Y).

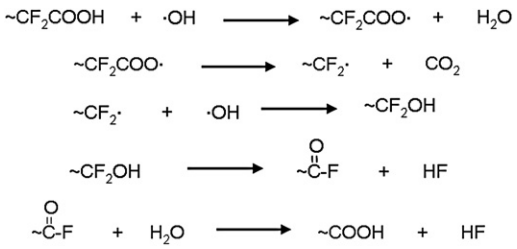

Scheme 3. Individual degradation reaction steps via end group unzipping.

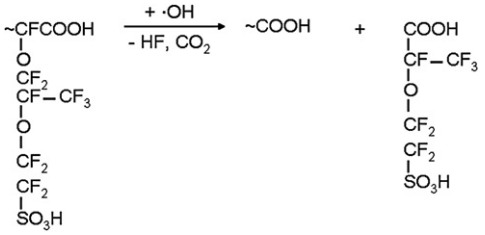

Scheme 5. Secondary degradation reaction via end group unzipping.

3.1.2. Degradation propagation via carboxylic acid end group unzipping

Once the carboxylic acid end groups are formed, the degradation proceeds via an unzipping reaction that involves a series of steps [1,4–7] demonstrated in Scheme 3. In Scheme 3, the attacking species may also involve other radical species besides the hydroxyl radicals (•OH) [10]. For ease of demonstration, however, we use the hydroxyl radical •OH to represent all possible attacking species, assuming that the other species react in a similar fashion as •OH and that all later kinetic discussion in this report is not affected by such a representation. Overall, each carboxylic acid end group reacts with two hydroxyl radicals to lose one CF_2 unit in the form of one carbon dioxide and two hydrogen fluoride molecules [1,4–7], as summarized in Scheme 4. The reaction represented in Scheme 4 occurs in a chain fashion to continue losing more CF_2 units from the polymer main chain [1,4–7].

Mechanistically, another degradation propagation reaction outlined in Scheme 5 should not be ignored. When the main chain end group unzipping reaction approaches the junction with the side chain, the side chain is cleaved from the polymer, producing HOOC–CF(CF_3)–O–CF_2CF_2–SO_3H [perfluoro(3-oxa-5-methyl)pentane-1-sulfonic-5-carboxylic diacid (molecule A)] [5,6,12]. On the main polymer backbone, a carboxylic acid end group is produced that would continue the main chain unzipping via the primary degradation reaction outlined in Scheme 4. Molecule A, meanwhile, can either diffuse out of the polymer membrane or continue its own degradation via similar unzipping reaction shown in Scheme 6. Overall, the complete degradation of molecule A leads to the formation of CO_2, HF, and sulfate ions.

3.1.3. Degradation initiation via side chain cleavage

Compared to the above weak end group initiation and main chain unzipping reactions via the carboxylic acid end groups, the degradation initiation via side chain cleavage is poorly understood both in terms of its occurrence under certain degradation conditions and the nature of the attacking species, if it does occur. We hereby assume that the side chain cleavage does occur. The reactions are expected to follow Scheme 7. In this scheme, X represents an unknown species that attacks the side chain. The location of the attack on the side chain is also unknown [1], as no definite evidence exists on the relative stability of the tertiary CF bond, the –C–O–C– ether bond, and the –C–SO_3H sulfonic acid link on the side chain under certain reaction conditions. Regardless of the exact location of the initial attack, however, a carboxylic acid group is expected to be produced, leaving behind the small molecular side chain fragments. Subsequently, the carboxylic acid group on the side chain unzips in the same way as shown in Scheme 4. The unzipping reaction eventually causes the main chain cleavage when it reaches the junction between the side chain and the main chain. As a result, the polymer main chain is cleaved and two carboxylic acid end groups are formed.

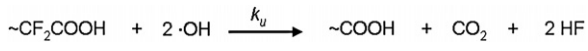

Scheme 4. Primary degradation reaction via end group unzipping.

3.2. Degradation kinetic considerations

The degradation mechanism outlined above allows us to develop a kinetic model with an emphasis on distinguishing the two initiation mechanisms: weak end group versus side chain cleavage. To do so, a series of assumptions and approximations are made.

For the end group initiation outlined in Scheme 2, we assume that this is a fast reaction – that is, the conversion of the unknown end groups Y into carboxylic acid end groups is complete at the very early stage of the overall PFSA degradation. This assumption is supported by the literature report that indeed typical non-perfluorinated end groups on fluorinated polymers are very vulnerable towards radical attack [9]. Fluoride ions may be produced in this reaction if Y contains fluorine atoms. The possible fluoride ions produced from this reaction are neglected in the following kinetic modeling; this approximation is justified based on the very low molar fraction of the end groups in the polymer, as a result of the typical high molecular weight of PFSA [13,14].

In terms of the production of carboxylic acid groups during the unzipping process, the primary unzipping degradation reaction (Scheme 4) does not produce additional carboxylic acid end groups. The secondary unzipping reaction (Scheme 5),

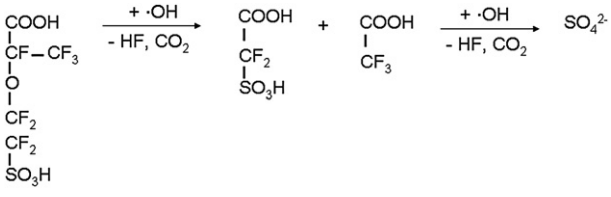

Scheme 6. Unzipping degradation reaction of molecule A.

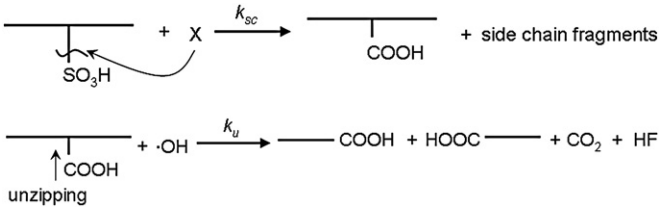

Scheme 7. Degradation initiation via side chain cleavage.

however, does produce molecule A which contains a carboxylic acid group in addition to the carboxylic acid end group remaining on the polymer main chain.

In principle, this additional carboxylic acid group on molecule A should be taken into account in terms of its contribution to the overall reaction kinetics. Practically, a fraction of molecule A may diffuse out of the membrane and should be considered inactive. For the fraction of molecule A that does remain in the membrane, it continues to degrade according to Scheme 6. On the one hand, the degradation of molecule A comes to completion within a few steps and the end products are CO_2, HF, and sulfate ions. In other words, the carboxylic acid group on any given molecule A is short-lived, compared to the carboxylic acid end groups on the polymer main chain which remain alive throughout the degradation process. On the other hand, molecule A is produced on a continuous basis as the degradation proceeds along the polymer main chain. The frequency of the occurrence of molecule A production from the main chain unzipping reaction is about once every 15 carbons on the main chain for Nafion® of EW of 1100. The combined effect of the low frequency of molecule A formation and its short lifetime is a deviation of the number of total carboxylic acid groups from that originating from the weak end groups, rather than a continuous increase of carboxylic acid groups. In other words, its steady state concentration approaches zero. It is important to note that this situation may change for Nafion® of much lower EW, in which case the production of molecule A may outweigh its consumption, leading to a continuous increase of carboxylic acids. For Nafion® of EW of 1100, we consider the only source for a continuous increase of the number of carboxylic acid groups to be the side chain cleavage reaction outlined in Scheme 7.

From the standpoint of fluoride ion production, both the main chain unzipping (Schemes 4 and 5) and the subsequent degradation of molecule A (Scheme 6) release fluoride ions. The number of fluorine atoms in molecule A is relatively small compared to that of the polymer main chain (plus the first two side chain fluorine atoms closest to the polymer main chain), with a ratio of 8:31 for Nafion® 1100. In other words, roughly 20% of the total fluorine in Nafion® 1100 is contained in molecule A. As molecule A further degrades according to Scheme 6, it produces $HOOC-CF_2-SO_3H$ and CF_3COOH. Both $HOOC-CF_2-SO_3H$ and CF_3COOH are small molecules; they can easily escape the system through either diffusion or evaporation (e.g. the boiling point of CF_3COOH is 78 °C, lower than the degradation temperatures often encountered). Indeed, this is supported by the experimental detection of CF_3COOH in fuel cell product water [6,12]. We believe that a portion of $HOOC-CF_2-SO_3H$ and molecule A itself may also diffuse out of the system, although we do not have experimental proof as to the extent of these losses due to diffusion. Overall, we believe that a large portion of fluorine atoms in molecule A does not end in the form of fluoride ions. Given the circumstance, the contribution of molecule A to fluoride ion production is expected to be significantly lower than the maximum possible 20% expected if all fluorine atoms in molecule A were converted into fluoride ions. As an approximation, we neglect the contribution of molecule A to the overall fluoride ion production in the following kinetic analysis.

Under the above assumptions and approximations, the main chain unzipping reaction (Scheme 4) and the side chain cleavage reaction (Scheme 7) are the only respective sources for the production of fluoride ions and additional carboxylic acid end groups. In addition, model compound studies reported in the literature suggest that the Nafion® side chains are much more stable than the carboxylic acid end groups [1,6,11,12]. The first reaction in Scheme 7 (attack by species X) is thus a slow reaction (assuming it does occur) compared to the unzipping reaction (the second reaction in Scheme 7). Kinetically, the first reaction is the rate-limiting step, and Scheme 7 is simplified as Scheme 8.

We note that Nafion® degradation occurs between the polymer in the solid phase and the attacking species in the gas phase (fuel cell and H_2O_2 flow cell) or liquid phase (Fenton's solution). To generalize, we define a fixed hypothetical volume V within which the concentration of the attacking species is (or are) uniformly distributed. The concentrations of the attacking species or functional groups on the polymer are thus the number of the species or functional groups divided by the hypothetical volume.

Based on Scheme 4, the rate of the end group unzipping is given by:

$$R_u = k_u \cdot [OH]^a \cdot [COOH] \quad (1)$$

where R_u: rate of the unzipping reaction; k_u: rate constant for the unzipping reaction; [OH]: concentration of •OH radicals; [COOH]: concentration of the carboxylic acid end groups on the polymer chains; a: reaction order with respect to •OH radicals.

In Eq. (1), we assume that the reaction order with respect to •OH radicals is a. The exact value of a depends on which one(s) of the reaction steps outlined in Scheme 3 is (are) the rate-limiting step(s). For instance, a should be equal to 1 if the first step is the rate-determining step, 2 if the first and third

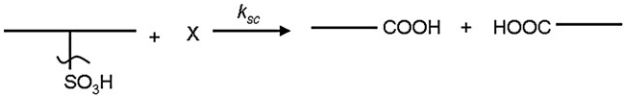

Scheme 8. Production of additional carboxylic acid end groups via side chain cleavage.

steps are both rate-limiting, and 0 if neither step 1 nor step 3 is the rate-limiting step. We simply assume a reaction order of a in the following kinetic analysis. As will become clear later in this paper, the exact value of a is irrelevant for this model.

Under the approximation that only the reaction in Scheme 4 contributes to fluoride ion production (i.e., the contribution of molecule A to fluoride production is ignored), the rate of fluoride ion production (or, equivalently, fluorine consumption from the polymer) according to Scheme 4 is expressed as:

$$\frac{\mathrm{d}\left([\mathrm{F}]_0-[\mathrm{F}]\right)}{\mathrm{d}t}=2R_\mathrm{u}=2k_\mathrm{u}\cdot[\mathrm{OH}]^a\cdot[\mathrm{COOH}], \tag{2}$$

where [F] represents the concentration of fluorine atoms retained on the polymer at time t and $[\mathrm{F}]_0$ is the concentration of fluorine atoms on the polymer at time 0.

We further define the fluorine loss fraction as L, with:

$$L=\frac{[\mathrm{F}]_0-[\mathrm{F}]}{[\mathrm{F}]_0}. \tag{3}$$

Combining Eqs. (2) and (3), we obtain:

$$\frac{\mathrm{d}L}{\mathrm{d}t}=\frac{\mathrm{d}\left([\mathrm{F}]_0-[\mathrm{F}]\right)}{[\mathrm{F}]_0\,\mathrm{d}t}=2k_\mathrm{u}\cdot[\mathrm{F}]_0^{-1}\cdot[\mathrm{OH}]^a\cdot[\mathrm{COOH}]. \tag{4}$$

From Scheme 8, the rate of the side chain cleavage reaction is expressed as Eq. (5). Based on the previous assumption that the reaction in Scheme 2 is a fast reaction (i.e., the weak end groups are completely converted into carboxylic acid in the very earliest stage of the overall degradation), the reaction in Scheme 8 is solely responsible for the formation of new carboxylic acid end groups and its rate can thus be expressed as Eq. (6),

$$R_\mathrm{sc}=k_\mathrm{sc}\cdot[\mathrm{X}]\cdot[\mathrm{S}] \tag{5}$$

$$\frac{\mathrm{d}[\mathrm{COOH}]}{\mathrm{d}t}=2R_\mathrm{sc}=2k_\mathrm{sc}\cdot[\mathrm{X}]\cdot[\mathrm{S}] \tag{6}$$

where R_sc: reaction rate for side chain cleavage; k_sc: reaction rate constant for side chain cleavage; [X]: concentration of reaction species X; [S]: concentration of the polymer side chain at time t; $[\mathrm{S}]_0$: initial concentration of polymer side chain ($t=0$).

Combining Eqs. (4) and (6), we obtain:

$$\frac{\mathrm{d}[\mathrm{COOH}]}{\mathrm{d}L}=\frac{k_\mathrm{sc}\cdot[\mathrm{X}]\cdot[\mathrm{S}]\cdot[\mathrm{F}]_0}{k_\mathrm{u}\cdot[\mathrm{OH}]^a\cdot[\mathrm{COOH}]}. \tag{7}$$

Based on our previous assumption that the side chain cleavage is a slow reaction compared to end group unzipping, we deduce that the predominant portion of the side chain loss is via the main chain end group unzipping reaction shown in Scheme 5, rather than the direct cleavage reaction in Scheme 8. In addition, Nafion® is a random copolymer of tetrafluoroethylene and the side chain-containing vinyl ether. Statistically, side chains are evenly distributed along the polymer main chain. Thus, the loss fraction for the side chain and fluorine should be equal. Eq. (3) can therefore be further extended to Eq. (8),

$$L=\frac{[\mathrm{F}]_0-[\mathrm{F}]}{[\mathrm{F}]_0}=\frac{[\mathrm{S}]_0-[\mathrm{S}]}{[\mathrm{S}]_0}, \tag{8}$$

which leads to Eq. (9),

$$[\mathrm{S}]=[\mathrm{S}]_0\cdot(1-L) \tag{9}$$

Substituting Eq. (9) into Eq. (7), we obtain:

$$\frac{\mathrm{d}[\mathrm{COOH}]}{\mathrm{d}L}=\frac{k_\mathrm{sc}\cdot[\mathrm{X}]\cdot[\mathrm{S}]_0\cdot[\mathrm{F}]_0}{k_\mathrm{u}\cdot[\mathrm{OH}]^a}\cdot\frac{(1-L)}{[\mathrm{COOH}]}. \tag{10}$$

Defining

$$\frac{k_\mathrm{sc}\cdot[\mathrm{X}]\cdot[\mathrm{S}]_0\cdot[\mathrm{F}]_0}{k_\mathrm{u}\cdot[\mathrm{OH}]^a}=C_1, \tag{11}$$

Eq. (10) becomes

$$\frac{\mathrm{d}[\mathrm{COOH}]}{\mathrm{d}L}=C_1\cdot\frac{(1-L)}{[\mathrm{COOH}]}. \tag{12}$$

In Eq. (11), $[\mathrm{S}]_0$ and $[\mathrm{F}]_0$ are dependent only on the polymer, and by definition are constants for a given polymer. k_u, k_sc, [X], [OH], and a are all dependent on the degradation conditions, including the type of degradation (Fenton's test, fuel cell, OCV, H_2O_2 flow cell, etc.), temperature of the degradation, and so forth. Under given constant degradation conditions, k_u, k_sc, [X], [OH], and a are all expected to remain constant (steady state assumption). Thus, C_1 would also be constant. We further define $k_\mathrm{sc}\cdot[\mathrm{X}]=k'_\mathrm{sc}$ and $k_\mathrm{u}\cdot[\mathrm{OH}]^a=k'_\mathrm{u}$, with k'_sc and k'_u being the respective apparent rate constants for the side chain cleavage and end group unzipping reactions. We therefore have:

$$C_1=\frac{k_{sc}\cdot[\mathrm{X}]}{k_\mathrm{u}\cdot[\mathrm{OH}]^a}\cdot[\mathrm{S}]_0\cdot[\mathrm{F}]_0=\frac{k'_\mathrm{sc}}{k'_\mathrm{u}}\cdot[\mathrm{S}]_0\cdot[\mathrm{F}]_0. \tag{13}$$

Eq. (13) reveals the physical meaning of C_1, which is that the value of C_1 is proportional to the apparent rate constants between side chain cleavage and main chain unzipping. For Eq. (12), it is equivalent to:

$$[\mathrm{COOH}]\cdot\mathrm{d}[\mathrm{COOH}]=C_1\cdot(1-L)\cdot\mathrm{d}L,$$

which on integration becomes

$$\int_{[\mathrm{COOH}]_0}^{[\mathrm{COOH}]}[\mathrm{COOH}]\cdot\mathrm{d}[\mathrm{COOH}]=C_1\cdot\int_0^L(1-L)\cdot\mathrm{d}L$$

with $[\mathrm{COOH}]_0$ being the initial concentration of carboxylic acid end groups on the polymer, which further leads to:

$$[\mathrm{COOH}]=\sqrt{[\mathrm{COOH}]_0^2+C_1\cdot L\cdot(2-L)}. \tag{14}$$

Eq. (14) is the most significant result of this kinetic modeling exercise. It quantitatively links the Nafion® fluorine fractional loss (L) and the concentration of the polymer carboxylic acid end groups [COOH] to C_1, which is proportional to the ratio of apparent rate constants between the side chain cleavage and the main chain unzipping reactions.

In the extreme, C_1 equals to 0 means that the side chain cleavage reaction does not occur. Eq. (14) then becomes:

$$[\mathrm{COOH}] = [\mathrm{COOH}]_0. \tag{15}$$

This equation implies that the concentration of the carboxylic acid end groups remains constant in the absence of the side chain cleavage initiation mechanism, which is consistent with our qualitative expectation.

3.3. Correlation of the end group measurement by infrared spectroscopy to the kinetic model

In principle, Eq. (14) allows us to calculate C_1 based on measured values of [COOH], $[\mathrm{COOH}]_0$, and L. Measuring L can be accomplished by either the conventional fluoride ion water analysis or an electron probe microanalysis (EPMA) method that we recently developed [15].

Quantitative measurement of the carboxylic acid end groups, however, is quite challenging, because of its very low fraction as the result of typical high molecular weights of Nafion [13,14]. Nevertheless, a method based on infrared (IR) analysis of membranes exchanged with metal ions has been used most often [5]. During the ion exchange process, small molecules such as molecule A are leached out of the membrane; thus, the IR method measures only the carboxylic acid groups attached to the polymer. Without knowing both the degraded membrane thickness and the molar extinction coefficients for the species of interest, the IR method does not measure directly the number of the carboxylic acid groups. Instead, it measures the relative number of carboxylic acid groups compared with the number of ether side chain groups. This is derived from the IR band ratio between 1691 cm^{-1} and 983 cm^{-1}, which correspond to the carboxylic acid potassium salt and the side chain ether C–O–C stretching bands, respectively. In effect, the IR band at 983 cm^{-1} is used as an internal reference for the analysis of the carboxylic acid end groups.

Based on Beer's law, we have:

$$A_{1691} = \varepsilon_{\mathrm{COOK}} \cdot b \cdot \left(N_{\mathrm{COOK}}/V_{\mathrm{p}}\right) \tag{16}$$

and

$$A_{983} = \varepsilon_{\mathrm{S}} \cdot b \cdot \left(N_{\mathrm{S}}/V_{\mathrm{p}}\right) \tag{17}$$

where A_{1691} and A_{983} are the IR peak absorbance values at 1691 cm^{-1} and 983 cm^{-1}, respectively. $\varepsilon_{\mathrm{COOK}}$ and ε_{S}: the molar absorptivities for the carboxylic acid potassium salt and the size chain, respectively; N_{COOK} and N_{S}: are the number of moles of the carboxylic acid potassium salt and the side chain in the polymer, respectively; and V_{p} is the volume of the dry polymer membrane.

Of course, the number of moles of the carboxylic acid potassium salt is equal to the number of moles of the carboxylic acid groups prior to the ion exchange. Therefore,

$$\frac{N_{\mathrm{COOK}}}{N_{\mathrm{S}}} = \frac{N_{\mathrm{COOH}}}{N_{\mathrm{S}}}, \tag{18}$$

with N_{COOH} and N_{S} representing the number of carboxylic acids and side chains on the polymer, respectively. With the earlier definitions of [COOH] and [S], we also have:

$$\frac{[\mathrm{COOH}]}{[\mathrm{S}]} \equiv \frac{N_{\mathrm{COOH}}/V}{N_{\mathrm{S}}/V} = \frac{N_{\mathrm{COOH}}/V_{\mathrm{p}}}{N_{\mathrm{S}}/V_{\mathrm{p}}} \equiv \frac{N_{\mathrm{COOH}}}{N_{\mathrm{S}}}. \tag{19}$$

From Eqs. (18), (19), and (9), we obtain

$$\frac{N_{\mathrm{COOH}}/V_{\mathrm{p}}}{N_{\mathrm{S}}/V_{\mathrm{p}}} = \frac{[\mathrm{COOH}]}{[\mathrm{S}]} = \frac{[\mathrm{COOH}]}{[\mathrm{S}]_0 \cdot (1-L)}. \tag{20}$$

Defining

$$R = \frac{A_{1691}}{A_{983}} \tag{21}$$

and substituting Eqs. (16), (17), and (20) into Eq. (21), we obtain:

$$R = \frac{\varepsilon_{\mathrm{COOK}} \cdot b \cdot N_{\mathrm{COOK}}}{\varepsilon_{\mathrm{S}} \cdot b \cdot N_{\mathrm{S}}} = \frac{\varepsilon_{\mathrm{COOK}}}{\varepsilon_{\mathrm{S}}} \cdot \frac{[\mathrm{COOH}]}{[\mathrm{S}]_0 \cdot (1-L)} = C_2 \cdot \frac{[\mathrm{COOH}]}{(1-L)}. \tag{22}$$

with

$$C_2 = \frac{\varepsilon_{\mathrm{COOK}}}{\varepsilon_{\mathrm{S}} \cdot [\mathrm{S}]_0}. \tag{23}$$

Eq. (22) is equivalent to Eq. (24),

$$[\mathrm{COOH}] = \frac{R \cdot (1-L)}{C_2}. \tag{24}$$

When $L = 0$, Eq. (24) becomes Eq. (25),

$$[\mathrm{COOH}]_0 = R_0/C_2. \tag{25}$$

Substituting Eqs. (24) and (25) into Eq. (14), we obtain:

$$\frac{R \cdot (1-L)}{C_2} = \sqrt{\left(\frac{R_0}{C_2}\right)^2 + C_1 \cdot L \cdot (2-L)}. \tag{26}$$

Squaring both sides of Eq. (26) and rearranging, we get:

$$R^2 = -C_1 \cdot C_2^2 + \left(R_0^2 + C_1 \cdot C_2^2\right) \cdot \left(\frac{1}{1-L}\right)^2. \tag{27}$$

In the absence of side chain cleavage (i.e., $C_1 = 0$), Eq. (27) becomes:

$$R = \frac{R_0}{1-L}. \tag{28}$$

Substituting Eqs. (13) and (23) into $C_1 \cdot C_2^2$, we have:

$$C_1 \cdot C_2^2 = \frac{k'_{sc}}{k'_u} \cdot [S]_0 \cdot [F]_0 \cdot \left(\frac{\varepsilon_{COOK}}{\varepsilon_S \cdot [S]_0}\right)^2 = \left(\frac{\varepsilon_{COOK}}{\varepsilon_S}\right)^2 \cdot \frac{[F]_0}{[S]_0} \cdot \frac{k'_{sc}}{k'_u}. \tag{29}$$

We further define:

$$C_i = \left(\frac{\varepsilon_{COOK}}{\varepsilon_S}\right)^2, \tag{30}$$

$$C_p = \frac{[F]_0}{[S]_0}, \tag{31}$$

and

$$C_k = \frac{k'_{sc}}{k'_u}. \tag{32}$$

Substituting Eqs. (30)–(32) into (29), we have

$$C_1 \cdot C_2^2 = C_i \cdot C_p \cdot C_k. \tag{33}$$

Based on their definitions (Eqs. (30)–(32)), C_i, C_p, and C_k are all unitless constants that are dependent on the infrared analysis conditions, the polymer structure, and the degradation reaction conditions, respectively.

For a given polymer, C_p can be calculated from the polymer structure. C_i can be determined by measuring the individual molar absorptivity using model compounds that mimic the chemical environment of the actual species. For polymers with the same structure and which are analyzed under the same infrared conditions, both C_i and C_p are constant. Thus, $C_1 \cdot C_2^2$ would be proportional to C_k based on Eq. (33). Under such a circumstance, determining C_i is not necessary for quantitative comparison of different degradation conditions and we consider its determination out of the scope of this paper.

3.4. Experimental validation of the model

Eq. (27) suggests that, for a given polymer degraded for different times under otherwise identical conditions, a plot of R^2 versus $1/(1-L)^2$ should yield a straight line with its slope and intercept equal to $R_0^2 + C_1 \cdot C_2^2$ and $-C_1 \cdot C_2^2$, respectively.

As for R_0, it refers to the R value of a non-degraded polymer within which all weak end groups are in the form of carboxylic acid. Practically, a non-degraded polymer always has some non-carboxylic acid weak end groups. Therefore, R_0 cannot be directly measured. However, Eq. (28) does suggest an experimental method to determine R_0: that is, in the absence of side chain cleavage, the measured R equals roughly to R_0 if L is small. As stated earlier in Section 1, there is sufficient evidence in the literature to suggest that under Fenton's test conditions, the dominant degradation mechanism is end group unzipping and the side chain cleavage is negligible [6,7]. Under such circumstance, R_0 can be determined by measuring the R value of Fenton's tested PFSA samples with insignificant weight loss.

Accordingly, a membrane sample was degraded under Fenton's test conditions listed in Section 2. The sample had a fluorine loss of 3% based on fluoride ions detected in the test solution by ion chromatography. After potassium ion exchange, an R value of 0.0228 was obtained by micro-IR analysis, resulting in a value of 0.00052 for R^2, which is taken as R_0^2.

For the two fuel cell-degraded MEA samples, their fluorine losses (L) were 12.2% and 28.0%, respectively, obtained by post-mortem electron probe microanalysis [15]. After ion-exchange, micro-IR spectra [16] were acquired for at least 10 different spots of each membrane sample. The representative infrared spectra of all the degraded membrane samples are shown in Fig. 1. The corresponding R values were obtained from the IR spectra and the average R values of all the measurements for the two fuel cell-degraded samples were 0.0520 and 0.0815, respectively.

The R^2 ($L = 0$) measured for the Fenton's test degraded sample and the R^2 values for the two fuel cell-degraded samples are plotted against $1/(1-L)^2$ in Fig. 2. A linear curve fitting results in the trend line in Fig. 2, with a standard deviation of 0.9981. The fact that the standard deviation is very close to 1 validates the kinetic model developed in this work. The

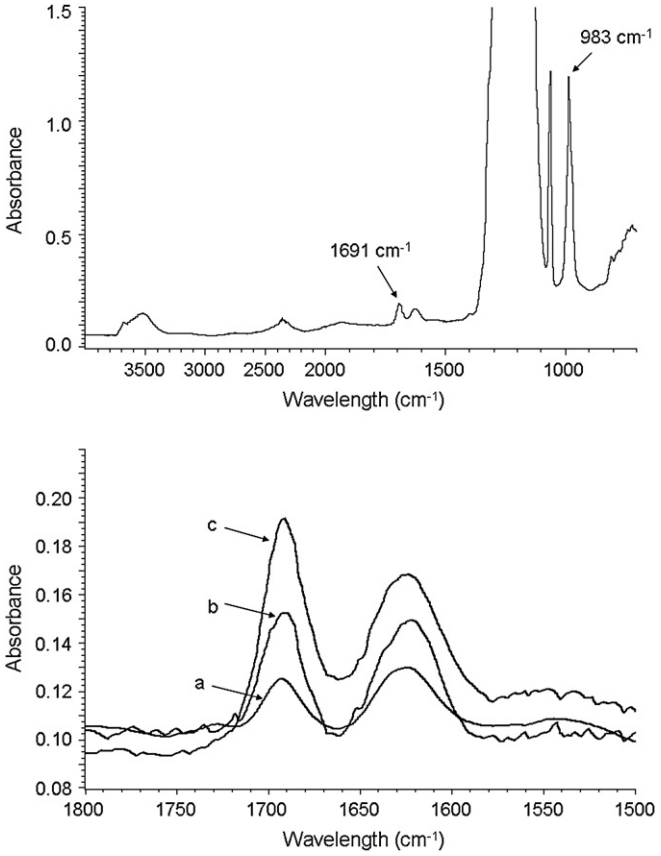

Fig. 1. Infrared spectra of K^+ ion exchanged degraded membranes. Upper: the full spectrum of the fuel cell-degraded membrane ($L = 28.0\%$); bottom: normalized carbonyl bands (1691 cm^{-1}) for three degraded membranes ((a) the Fenton's degraded sample; (b) the fuel cell-degraded sample with $L = 12.2\%$; (c) the fuel cell-degraded sample with $L = 28.0\%$).

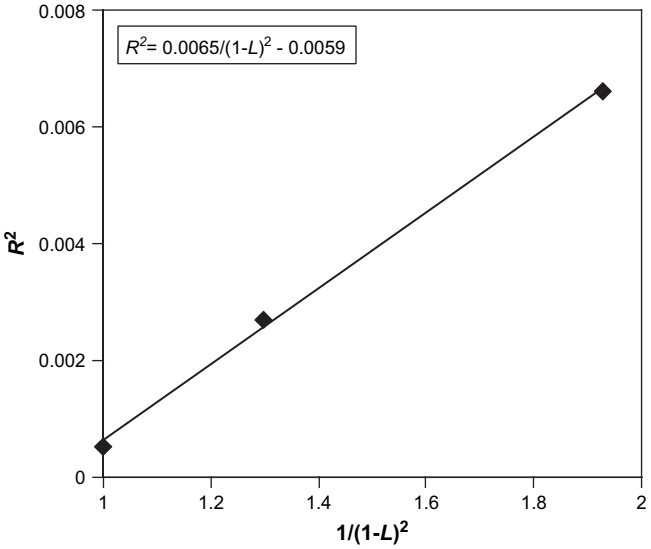

Fig. 2. Determination of $C_1 \cdot C_2^2$ and R_0^2.

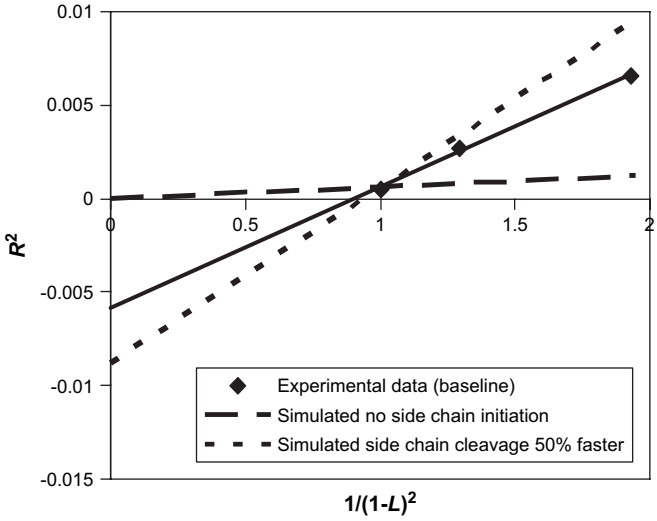

Fig. 3. Effect of the extent of side chain cleavage.

slope and intercept of the fitted linear line are 0.0065 and −0.0059, respectively. Based on Eq. (27), we obtain the value of 0.0059 for $C_1 \cdot C_2^2$ and the value of 0.0006 for R_0^2, the latter of which is in good agreement with the assumed R_0^2 from the Fenton's tested sample (0.00052).

As stated earlier, Eq. (33) suggests that, for degraded polymer samples possessing the same chemical structure and analyzed under the same infrared analysis conditions, $C_1 \cdot C_2^2$ is linearly proportional to C_k. Essentially, Eqs. (27) and (33) establish the basis to experimentally quantify C_k, which is the ratio between the apparent rate constant of the side chain cleavage reaction and that of the main chain end group unzipping reaction.

3.5. Applicability of the kinetic model

The data in Fig. 2 demonstrate the validity of the kinetic model established in this work. We note that this kinetic model is based on the unique mechanism by which PFSA polymers degrade. Thus, it is not applicable to ionomers which degrade via an entirely different mechanism, such as hydrocarbon ionomers. The usefulness of the kinetic model can be realized by extending this model to PFSA polymers degraded under a variety of conditions. By doing so, quantitative knowledge can be obtained on how polymer degradation conditions (e.g. fuel cell operating conditions such as temperature, humidity, etc.) affect the two degradation initiation mechanisms (weak end group vs. side chain cleavage). In the following section, we demonstrate the applicability of the kinetic model under a variety of scenarios.

For illustration purposes, the experimental data and fitted curve in Fig. 2 were replotted in Fig. 3 for use as the baseline. The fitted baseline curve in Fig. 3 was extrapolated to $1/(1-L)^2 = 0$ in order to visually illustrate the Y-intercept value of $C_1 \cdot C_2^2$ ($R^2 = -C_1 \cdot C_2^2$ when $1/(1-L)^2 = 0$). We note that L represents the fractional loss of fluorine, the value of which should be in the range of 0–1. Accordingly, the value of $1/(1-L)^2$ is in the range between 1 and ∞. In the analysis that follows, the value of $1/(1-L)^2$ below 1 is therefore practically inaccessible, but mathematically meaningful for obtaining the kinetic constant $C_1 \cdot C_2^2$.

3.5.1. Side chain cleavage versus weak end group initiation

For the same PFSA polymer degraded under different conditions and analyzed under the same infrared conditions, C_i and C_p are identical. The extent of the side chain cleavage initiation reaction (Scheme 8) relative to the weak end group initiation (Scheme 2) (C_k) is directly reflected in $C_1 \cdot C_2^2$ based on Eq. (33).

Since, in the current discussion, the polymer structure including the end groups is the same, R_0 remains unchanged. We assume three different scenarios:

(1) No side chain cleavage initiation, only weak end group initiation:

$C_1 \cdot C_2^2 = 0$, $R_0^2 = 0.0006$ (the baseline value), Eq. (27) becomes:

$$R^2 = 0.0006/(1-L)^2. \tag{34}$$

(2) No weak end group initiation, only side chain cleavage initiation:

$C_1 \cdot C_2^2 = \infty$, $R_0^2 = 0.0006$, the slope in Eq. (27) is equal to infinity. Since all end groups become stable, k_u is equal to 0 and Eq. (7) and all the subsequent equations become meaningless. In this case, the kinetic model is not applicable. In reality, the number of PFSA polymer weak end groups can be significantly reduced by polymer post-treatment [7], but the complete removal of weak end groups is nearly impossible from a synthetic chemistry standpoint.

(3) Side chain cleavage 50% faster:

$C_1 \cdot C_2^2 = 0.0059 \times 1.5 = 0.0089$, $R_0^2 = 0.0006$. According to Eq. (27), Eq. (35) is obtained:

$$R^2 = 0.0095/(1-L)^2 - 0.0089. \quad (35)$$

Eqs. (34) and (35) are used to generate the two simulated curves in Fig. 3, respectively. All three curves in Fig. 3 meet at $1/(1-L)^2 = 1$ since R_0^2 is the same. With values of R^2 at $1/(1-L)^2 = 0$ and the slopes equal to $-C_1 \cdot C_2^2$ and $(R_0^2 + C_1 \cdot C_2^2)$, respectively, the slope increases and the intercept at $1/(1-L)^2 = 0$ decreases when more and more severe side chain cleavage initiation occurs relative to the amount of weak end group initiation.

3.5.2. Impact of polymer structure

Assuming that the degradation conditions and infrared analysis conditions remain constant (i.e., both C_i and C_k remain unchanged), we illustrate below the impact of PFSA polymer structures on both R_0^2 and $C_1 \cdot C_2^2$.

(1) Reducing the polymer molecular weight by 50% (or doubling the number of weak end groups):

Combining Eqs. (23) and (25), we obtain:

$$R_0 = \frac{\varepsilon_{COOK}}{\varepsilon_S} \cdot \frac{[COOH]_0}{[S]_0}. \quad (36)$$

In Eq. (36), halving the molecular weight increases the $[COOH]_0$ by a factor of two. This has the effect of doubling R_0, based on Eq. (36). This change does not impact C_i, C_p, and C_k based upon their definitions (Eqs. (30)–(32)); therefore, $C_1 \cdot C_2^2$ remains unchanged. Using the baseline R_0^2 and $C_1 \cdot C_2^2$ values, the values corresponding to this change are: $R_0^2 = 0.0006 \times 2^2 = 0.0024$, $C_1 \cdot C_2^2 = 0.0059$. This would lead to:

$$R^2 = 0.0083/(1-L)^2 - 0.0059. \quad (37)$$

Instead of reducing the molecular weight, doubling the number of weak end groups on the same molecular weight polymer would result in the same outcome and is completely equivalent. This impact of reducing the polymer molecular weight by 50% or doubling the number of weak end groups is further demonstrated in the R^2 versus $1/(1-L)^2$ curve simulated using Eq. (37) (shown in Fig. 4 along with the baseline curve).

(2) Increasing polymer EW by 20%:

In developing our kinetic model, we assumed that the contribution of molecule A to the formation of both new carboxylic acid end groups and fluoride ions was negligible. The validity of these two assumptions depends on the EW of the polymer, which in the baseline case is 1100. Any increase in EW should not impact the validity of these assumptions, but significant reduction of EW may. We hereby assume a case with a polymer of EW 20% higher than the baseline case. This increase in EW leads to a 20% reduction in the number of side chains $[S]_0$. According to Eq. (36), R_0 increases by 20%. The new value of R_0^2 is thus equal to $0.0006 \times (1+20\%)^2 \approx 0.0009$. Based on the definition of C_p (Eq. (31)), such a reduction of $[S]_0$ leads to the increase of C_p by 20%. Since C_i and C_k remain unchanged, $C_1 \cdot C_2^2$ also increases by 20% to $0.0059 \times (1+20\%) = 0.0071$. Inputting the new values R_0^2 of $C_1 \cdot C_2^2$ into Eq. (27), we obtain:

$$R^2 = 0.0080/(1-L)^2 - 0.0071. \quad (38)$$

Once again, a curve is simulated using Eq. (38) and plotted in Fig. 4, which shows that both R_0^2 of $C_1 \cdot C_2^2$ change as a result of increasing the polymer EW.

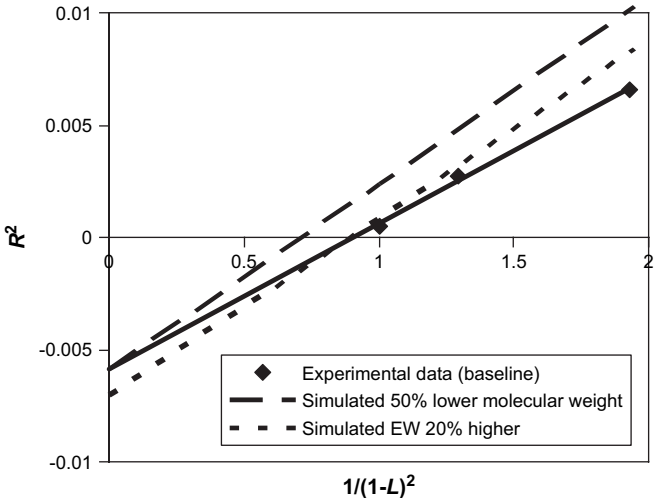

Fig. 4. Effect of polymer structure.

The above theoretical case study shows how knowledge about the degradation mechanism can be extracted from the kinetic model established in this work. The case study on the impact of polymer structure reminds us that special care must be taken when comparing PFSA polymers of different structures. By applying the kinetic model to future experimental data, knowledge can be gained to guide us in how best to improve the durability of PFSA-based PEM by either operating fuel cells under conditions which minimize the side chain cleavage reaction or designing new PFSA polymers with more stable side chains.

4. Conclusions

PFSA chemical degradation in various degradation environments proceeds via the same carboxylic acid end group unzipping mechanism. These carboxylic acid end groups can originate from the weak polymer end groups and/or the side chain cleavage reaction, depending on the specific degradation conditions. These two degradation initiation mechanisms are difficult to distinguish for PFSA degradation in fuel cells, due to the system complexity. In this paper, the PFSA chemical degradation reaction mechanism and kinetics are reviewed. Under a series of carefully considered assumptions and approximations, Eqs. (14), (27), and (33) are obtained which quantitatively distinguish the side chain cleavage and

the main chain carboxylic acid unzipping reactions. Infrared spectroscopy was used to measure the carboxylic acid end groups of degraded polymers. The IR data (R) coupled with the ionomer fluoride loss data (L) validate the kinetic model, and the corresponding kinetic constant $C_1 \cdot C_2^2$ is obtained. Theoretical case studies based on Eqs. (27) and (33) are conducted to illustrate the usefulness of the kinetic analysis. The kinetic model established in this work can be used as a universal tool to elucidate the PFSA chemical degradation mechanism in various degradation environments including fuel cells. The benefit of this work can and will only be realized by extending the kinetic model to PFSA polymers degraded under various conditions (e.g. fuel cell operating conditions). Ultimately, the potential impact of this work lies in providing guidance in improving PFSA durability through purposeful molecular design of new PFSA materials or operating fuel cells under favorable conditions.

Acknowledgement

The authors thank the following General Motors colleagues: Dr. Hubert Gasteiger for his thoughtful comments and suggestions, Dr. Tim Fuller for providing degraded polymer samples, and Mrs. Deborah Eckel at GM R&D for her assistance in IR measurement.

References

[1] Schiraldi DA. Polym Rev 2006;46(3):315.
[2] Doyle M, Rajendran G. In: Vielstich W, Lamm A, Gasteiger H, editors. Handbook of fuel cells, vol. 3. Chichester, England: John Wiley & Sons; 2003. p. 351.
[3] Rikukawa M, Sanui K. Prog Polym Sci 2000;25(10):1463.
[4] (a) LaConti AB, Handan M, McDonald RC, Vielstich W, Lamm A, Gasteiger H, editors. Handbook of fuel cells, vol. 3. Chichester, England: John Wiley & Sons; 2003. p. 647;
(b) Kinumoto T, Inaba M, Nakayama Y, Ogata K, Umebayashi R, Tasaka A. J Power Sources 2006;158:1222.
[5] Hommura S, Kawahara K, Shimohira T. Poster #803, 207th meeting of the Electrochemical Society, Quebec City, Canada; 15–20 May 2005.
[6] (a) Xie T, Hayden CA, Healy J, Olson KL. Chemical degradation of perfluorinated sulfonic acid ionomer. Adv. Mater. Proton exchange membrane fuel cell systems conference, Pacific Grove, CA; February 2005. p. 24;
(b) Healy J, Hayden C, Xie T, Olson K, Waldo R, Brundage M, et al. Fuel Cells 2005;5:302.
[7] Curtin DE, Lousenberg RD, Henry TJ, Tangeman PC, Tisak ME. J Power Sources 2004;131:41.
[8] Xie J, Wood III DL, Wayne DM, Zawodzinski TA, Atanassov P, Borup RL. J Electrochem Soc 2005;152(1):A104.
[9] Pianca M, Barchiesi E, Esposto G, Radice S. J Fluorine Chem 1999;95:71.
[10] Kadirov MK, Bosnjakovic A, Schlick S. J Phys Chem 2005;B109(16):7664.
[11] Schiraldi DA, Zhou C, Zawodzinski TA. Chemical durability studies of PFSA polymers and model compounds under mimic fuel cell conditions. 203th American Chemical Society National Meeting, Washington, DC; August 2005. Paper Fuel 43.
[12] Schwiebert K, Raiford K, Nagarakan G, Principe F, Escobedo G. Strategies to improve the durability of perfluorosulfonic acid membranes for PEM fuel cells. KFTCA International Symposium, Washington, DC; December 2005.
[13] Fernandez RE. In: Mark JE, editor. Polymer data handbook. New York: Oxford University Press; 1999.
[14] Mauritz KA, Moore RB. Chem Rev 2004;104(10):4535.
[15] Xie T, Waldo RA. Manuscript in preparation.
[16] Due to the interference of the catalyst layer, typical macro-IR methods employed in the literature were found to be ineffective; a micro-IR method was thus developed and used. Hayden CA, Eckel D, Xie T. unpublished results.